Analysis of Self-Pulsating Three-Section DBR Lasers

Paolo Bardella and Ivo Montrosset, *Member, IEEE*

***Abstract*—The characteristics of a three-section distributed Bragg reflector laser showing self-pulsation have been analyzed using a large signal time-domain traveling-wave simulator. The device dynamic properties have been investigated in all their complexity and analyzed as functions of the linewidth enhancement factor and of the injected current in the active and in the phase control sections. The simulation results have clearly shown the fundamental role of four wave mixing on the laser characteristics (output power, spectrum, etc.) and have been quantitatively correlated with the few available theoretical and experimental results. The considered self-pulsation operation frequencies around 40 GHz are of interest for practical applications.**

***Index Terms*—Distributed Bragg reflector (DBR) lasers, multisection laser, self-pulsation, stability.**

I. Introduction

THE development and the diffusion of broadband optical connections and the reduction of the costs to the final customer will cause in the next few years a dramatic growth in Internet traffic. In this scenario, that requires very high speed communication systems, all-optical processing functions such as clock recovery, and retiming, reshaping, and reamplification (3R), will play a leading role. Many types of self-pulsating (SP) lasers have been analyzed for these purposes [1]–[3].

The most used and analyzed integrated SP sources are the multisection distributed feedback (DFB) lasers built as two detuned DFBs separated by a passive phase-control section [1], [4], [5] and the multisection gain-coupled DFB [3], [6]. More recently, integrated DFBs with passive or active feedback have also been studied [7], as well as sampled grating DFBs [8].

A simpler yet effective alternative to these laser configurations is represented by the three-section (3S) distributed Bragg reflector (DBR) laser (Fig. 1). Tuning the dc currents injected in the active and the phase control sections, it is possible to obtain in-phase beating of adjacent modes around the frequency selected by the grating and thus an oscillating optical output power. The main advantage of this solution consists in its simplicity and easy fulfillment. Recently, SP-3S DBRs have been realized [9], proving that these simple devices can be candidates for clock-recovery systems. A theoretical model of the mechanism that generates self-pulsation has been proposed in [10]. This model, based on small signal analysis, indicates that the longitudinal modal coupling generated by the four-wave mixing (FWM) effect is responsible for SP. In this paper we present, with a broader analysis than in [10], the different working conditions of a SP-3S DBR laser. To perform this analysis, we used the time-domain traveling waves method presented in [11]. With this numerical approach, we were able to observe all the quantity of interest (optical fields, carrier densities, gain, etc.) and thus have a deep understanding of the physical phenomena by a proper processing of the simulator results. In Section II, we will briefly present the foundation of the numerical model that is able to simulate a wide variety of optical devices. In Section III, we will analyze the DBR self-pulsation conditions. Starting from the $P-I_a$ characteristics, we will show that DBR lasers can exhibit sudden transitions from SP regions to continuous-wave (CW) regimes and *vice versa*. The laser output spectrum respect to grating reflectivity and the effect of changing the Henry factor show how FWM plays a fundamental role in determining self-pulsation. Furthermore the simulation results have been processed in order to extract fundamental information on the laser dynamic from the maps of the time evolution of carrier density versus instantaneous frequency.

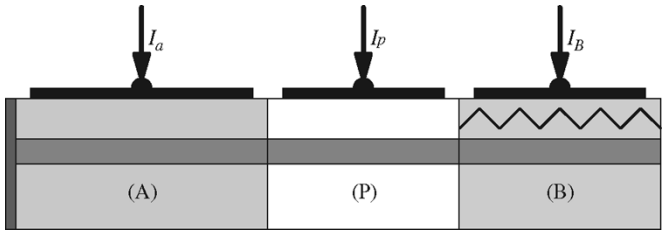

Fig. 1. Schematic of a 3S DBR laser with active region (A), phase control region (P), and Bragg reflector (B).

II. Numerical Model

Our model is based on the time-domain traveling-wave equations. We just consider the slowly varying components of the electric fields, so that the total electric field in the cavity can be expressed as

$$E(z,t)=\left(F(z,t)e^{-\frac{j\pi z}{\Lambda}}+R(z,t)e^{\frac{j\pi z}{\Lambda}}\right)e^{j\omega_0 t}$$

where Λ is the grating section pitch and $\omega_0=2\pi c/\lambda_B$, where λ_B has been chosen to be the grating Bragg wavelength. The forward (F) and reverse (R) traveling waves in the cavity are normalized in order to calculate the photon density S as $|F|^2+|R|^2$. The two equations for the electric fields are coupled with the carrier density (N) rate equation, yielding the system

$$\begin{cases}\left(\frac{1}{v_g}\frac{\partial}{\partial t}+\frac{\partial}{\partial z}\right)F(z,t)=-\left(j\delta(z,t)-\Gamma g(z,t)+\alpha_l\right)F(z,t)\\ \qquad\qquad +j\kappa R(z,t)+S_{\rm sp}\\ \left(\frac{1}{v_g}\frac{\partial}{\partial t}-\frac{\partial}{\partial z}\right)R(z,t)=-\left(j\delta(z,t)-\Gamma g(z,t)+\alpha_l\right)R(z,t)\\ \qquad\qquad +j\kappa F(z,t)+S_{\rm sp}\\ \frac{d}{\mathrm{d}t}N(z,t)=\frac{I_a}{ewdl_a}-\frac{N(z,t)}{\tau}-v_g\frac{\Gamma g(z,t)}{1+\varepsilon S(z,t)}S(z,t)\end{cases} \quad (1)$$

Manuscript received July 28, 2004; revised December 13, 2004. This work was supported in part by the Italian Ministry of Education (MIUR) in the framework of the research project "Transmission on very high bit rate OTDM systems."

The authors are with the Dipartimento di Elettronica and PhotonLab, Politecnico di Torino, Torino 10129, Italy (e-mail: ivo.montrosset@polito.it).

Digital Object Identifier 10.1109/JSTQE.2005.845608

TABLE I
PARAMETER VALUES

Symbol	Meaning	Value	Unit
	Active region		
$l_{\rm a}$	Length	790	μm
w	Width of the active layer	0.6	μm
d	Thickness of the active layer	0.4	μm
a	Linear gain coefficient	$2.3\,10^{-16}$	$\rm cm^{-2}$
γ	Gain maximum wavelength	1.55	μm
Γ	Confinement factor	0.58	
$\alpha_{\rm l,a}$	Material losses	1.5	$\rm cm^{-1}$
$n_{\rm eff,0}$	Refractive index	3.4	
A	Monomolecular recomb. coeff.	$3\,10^{8}$	$\rm s^{-1}$
B	Bimolecular recomb. coeff.	10^{-10}	$\rm cm^3 s^{-1}$
C	Auger recombination coeff.	10^{-29}	$\rm cm^6 s^{-1}$
N_0	Carrier density at transparency	10^{18}	$\rm cm^{-3}$
$\beta_{\rm sp}$	Spontaneous emission factor	10^{-6}	
ε	Gain compression factor	$0.1\,10^{-17}$	$\rm cm^3$
	Phase control region		
$l_{\rm p}$	Length	130	μm
$\alpha_{\rm l,p}$	Material losses	1	$\rm cm^{-1}$
$\rm n_{eff,0}$	Refractive index	3.4	
τ_p	Carrier lifetime	$5\,10^{-9}$	s
	Bragg reflector region		
$l_{\rm r}$	Length	200	μm
$\alpha_{\rm l,r}$	Material losses	5	$\rm cm^{-1}$
$\rm n_{eff,0}$	Refractive index	3.4	
$\lambda_{\rm B}$	Bragg wavelength	1.55	μm
κ	Coupling coefficient	40	$\rm cm^{-1}$

In the active section, we consider a linear dependence of the gain maximum with the carrier density $g(z,t) = a(N(z,t) - N_0)$, whereas we use a digital filter to include the variation of the gain with the bandwidth [12]. The variation of the effective refractive index with the carrier density has been represented as

$$n_{\rm eff}(z,t) = n_{\rm eff,0} - c\frac{\alpha_H}{2\omega_0}\Gamma a\,(N(z,t) - N_0)$$

whereas Γ is the transverse optical confinement factor and α_H is the Henry linewidth enhancement factor. The detuning term $\delta(z,t)$ is calculated as

$$\delta(z,t) = \frac{\omega_0}{c} n_{\rm eff}(z,t) - \frac{\pi}{\Lambda}$$

and $S_{\rm sp}$ is the spontaneous emission term. The remaining undefined parameters in (1) are listed in Table I.

To numerically evaluate the system of nonlinear differential equations (1), we use the split-step algorithm [11]. The benefits of this model are its simplicity, reliability, and high computational speed.

The device we studied is similar to the SP-3S DBR experimentally measured by [9]; the parameters value we used are reported in Table I.

III. ANALYSIS OF SP CONDITIONS

From a numerical point of view, the determination of SP conditions in a 3S DBR was not an easy task because we had to properly choose the device and material parameters and then find the suitable bias conditions. Material parameters as well as cavity operating conditions strongly influence the output signal and in our case the SP. The best SP operations are quite difficult to determine because from our analysis we found SP as a condition where two or more modes are in competition and phase-locked by the mode coupling produced by FWM.

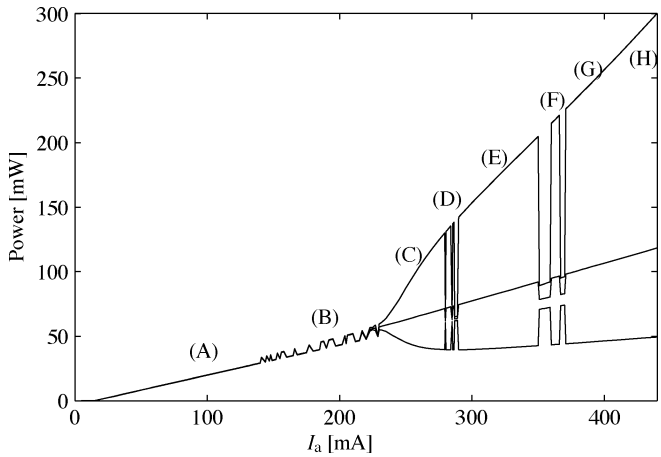

Fig. 2. $P - I_a$ curve of the SP-3S DBR when $\alpha_H = 4$ and for the parameters in Table I. The three curves indicate the maximum, the mean and the minimum output power. (A) CW operating region. (B) CW bistable region. (C), (E), (G) SP regions. (D), (F) Transition between different SP behavior. (H) Irregular behavior.

For this reason, in this section we first of all present how SP conditions have been found by computing the $P - I_a$ characteristic at constant phase and grating sections bias currents with a set of properly selected cavity and material parameters. After discussing the various operating conditions in the $P - I_a$ characteristic and how they change varying the material parameters, we present the effect of the fine-tuning by current injection in the phase section (I_p in Fig. 1). Furthermore the dynamic behavior has been analyzed by inspection of the laser dynamic in the carrier density-instantaneous frequency plane.

A. SP 3S DBR $P - I_a$ Characteristics

We first calculated the optical power versus active section current $(P - I_a)$ characteristic of a device described in Table I with $\alpha_H = 4$. The simulated $P - I_a$ characteristic has been obtained by switching on the laser for each considered current value and by analyzing the obtained steady state output power. The results are presented in Fig. 2, where we report the maximum, the average, and the minimum values extracted from the temporal evolution of the output power for the structure in Fig. 1 and with the parameter values defined in Table I. We found the threshold current at 16 mA; the CW power increases linearly up to 130 mA (region (A) in Fig. 2), where a bistability region begins [region (B)]. In this region, the steady state power is always constant, but if we repeat the simulation with different values of the initial noise, the laser can work in one of the two stable CW conditions.

For currents higher than 230 mA [regions (C) and (E)], self-pulsations start growing. Their increase is not continuous with the injected current: for I_a around 280 mA [region (D)] and 360 mA [region (F)], the oscillations are much more reduced. We indeed observe only a slight separation between maxima and minima of output powers. These regions correspond to transitions to different SP behaviors. Self-pulsations start growing in region (G) but become irregular for currents higher than 400 mA [region (H)]. The experimental evidence of both bistable and SP regions in a DBR laser characteristic was first reported in [13].

From the computed output field, we numerically evaluated the optical spectrum to better understand the evolution of the system operating conditions. The temporal evolution of the steady state

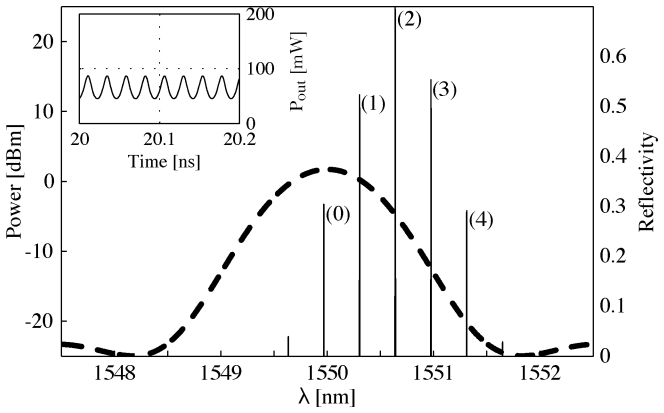

Fig. 3. Optical spectrum for the laser in the first SP region (region (C), Fig. 2). Grating power reflectivity with $\lambda_B = 1550$ nm: dashed line. In the insert: instantaneous output power. SP frequency of 41.58 GHz.

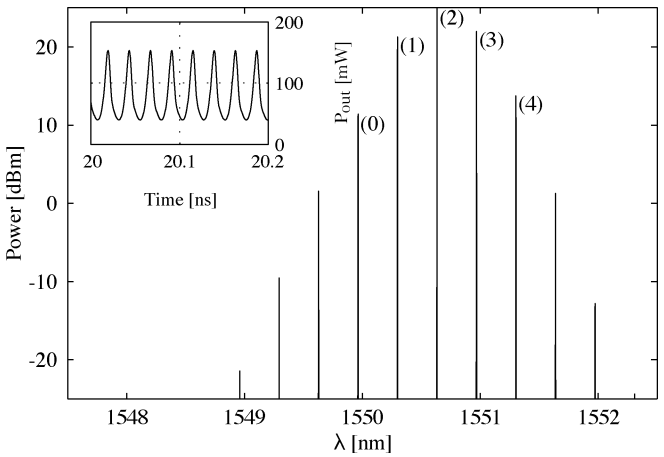

Fig. 4. Same as Fig. 3, but with $I_a = 300$ mA (region (E) in Fig. 2). SP frequency of 41.74 GHz. The spectral power distribution is in good agreement with the experimental results in [9].

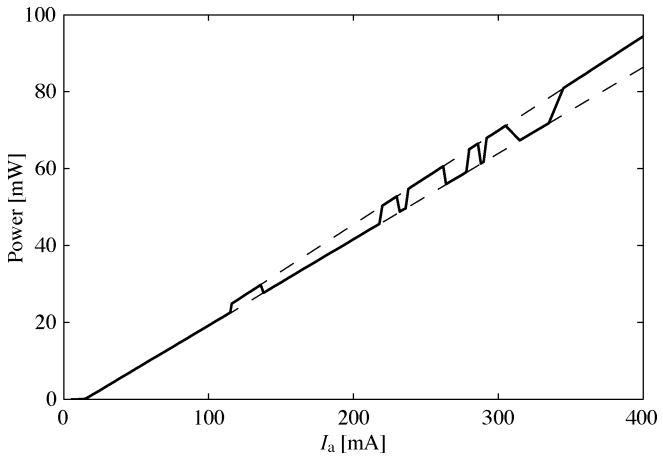

Fig. 5. $P - I_a$ curve as in Fig. 2 when $\alpha_H = 2$. Bistable behavior for $I_a > 110$ mA. Dashed lines: bistability loop.

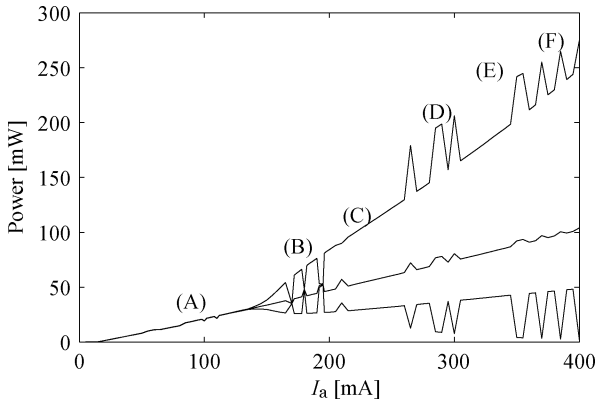

Fig. 6. $P - I_a$ curve as in Fig. 2 when $\alpha_H = 6$. (A) CW operating region, (C, E) SP regions, (B, D, F) transitions between SP regions.

computed field was first multiplied by a Hann window (to reduce spectral leakage [14]), and then the discrete Fourier transform was calculated. The optical spectrum of SP occurring when $I_a = 250$ mA is reported in Fig. 3. It is paramount to observe the red shift of the lasing optical spectrum respect to the grating reflectivity spectrum. This condition is typical of a laser with significant FWM effect [15]–[18]. The same consideration applies for the SP behavior at $I_a = 300$ mA (see Fig. 4).

When the device is SP, we can also remark that mode 3 in Figs. 3 and 4 has a higher power than mode 1 (their difference is about 1.5 dBm). This result reflects quantitatively what was indicated in [10] as a fundamental requirement to obtain self-pulsation via FWM effect. The spectrum in Fig. 4 is in quantitative agreement with the experimental results in [9].

Been the coupling between longitudinal modes due to FWM proportional to $(1 + i\alpha)$ [19]–[22], in order to prove the FWM fundamental role we repeated the same simulations for different values of the linewidth enhancement factor. For $\alpha_H = 2$, we did not find self-pulsations but only a bistable behavior even for high currents (Fig. 5). If, on the contrary, we increase α_H up to six, self-pulsations start at lower currents (Fig. 6). In regions (D) and (F), we found that the laser is bistable again but with another form of bistability: the laser is still SP, but the emission spectrum is different for the two states.

A second effect we analyzed is the impact of the gain saturation coefficient ε on the $P - I_a$ characteristics. For the case with $\alpha_H = 4$ we doubled its value to $\varepsilon = 0.2\ 10^{-17}$ cm^3. We found the self-pulsation to start earlier, at $I_a = 80$ mA, and the transition to irregular pulsations (like region (F) in Fig. 2) occurs for $I_a \simeq 150$ mA. We observed a reduction of the SP current interval in respect to the case in Fig. 1. We attributed this reduction to an increased variation of the carrier density due to the optical power that faster shifts the lasing mode frequency respect to the case with low saturation.

To further analyze the laser dynamic behavior, we isolated by numerical filtering each spectral line and we recovered its temporal evolution calculating the inverse Fourier transform. Numerical calculations show that in SP behaviors the power associated with each lasing mode is constant, and so is the phase difference between adjacent modes. On the contrary, when the laser is monomodal or not SP, the phase between the lasing modes is rapidly varying in time.

The general complex behavior we described for the $P - I_a$ characteristics can be interpreted in the following way: while the current increases, more power is transferred via FWM to modes having higher wavelengths; in Fig. 1, region (B), the coupling between modes is not yet strong enough to generate self-pulsations, so only one mode is lasing. When I_a reaches a sufficient value, the power transfer between the modes due to FWM

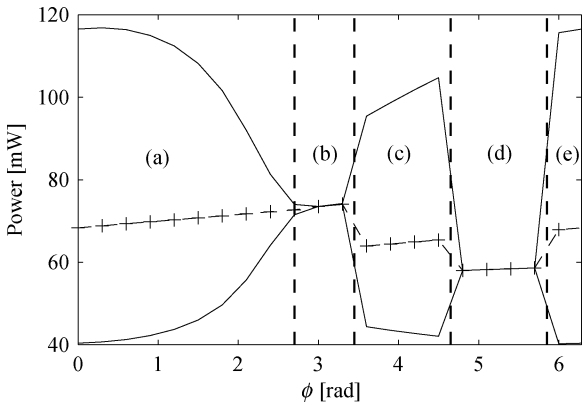

Fig. 7. Maximum, average and minimum output power as functions of the total phase variation. In (a), (c) and (e), the laser is SP; in (b) and (d), it is monomode.

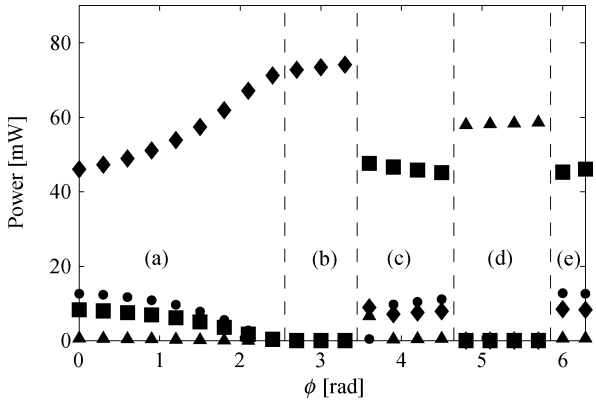

Fig. 8. Mode output power for the case in Fig. 6 (▲: mode 0, ■: mode 1, ♦: mode 2, • mode 3, following the numbering introduced in Fig. 3).

is higher, allowing the other modes to laser, thus allowing the self-pulsations to grow [region (C)].

B. Effect of Fine-Tuning on Self-Pulsations

The next step in our analysis has been to investigate the influence on the SP behavior of the lasing modes position with respect to the maximum of the grating reflectivity. This can be experimentally done by current injection in the phase control section, changing the waveguide effective refractive index and therefore the phase of the optical field propagating in this section. In our case, a change of the effective index of 0.0059 shifts the modes of one free-spectral range (FSR). To model this change due to current injection in an easy way, we introduced a normalized parameter, the phase shift ϕ, ranging from 0 to 2π. ϕ represents the phase variation, with respect to zero current injection, of the electric field propagating for a length l_p in the phase section. We selected in this phase interval 22 points and, after choosing an operation point on the $P - I_a$ characteristic, we evaluated P versus ϕ (normalized tuning current I_p) curves.

In Fig. 7, as in the previous $P - I_a$ curves, the maximum, the average, and the minimum powers are reported as functions of ϕ for the case when $\alpha_H = 4$ and $I_a = 269$ mA. In these results, it is possible to define five operating regions: in region (a), the device is SP and the ratio between the maximum and minimum power reduces while increasing ϕ, until the device becomes monomodal [region (b)]. Then, suddenly, the self-pulsation appears again in region [region (c)] but, after a small phase interval, the operation is again monomodal [region (d)]. When $\phi \simeq 2\pi$, the SP starts again [region (e)], thus connecting with continuity the characteristic to the values assumed when $\phi = 0$. The powers associated with the most relevant modes during tuning have been calculated and are reported in Fig. 8.

For a better understanding of the results, in Fig. 9 we reported also the operation wavelengths of the most relevant lasing modes versus ϕ, using the numbering previously introduced in the spectrum with zero tuning current (Figs. 3 and 4). In region (a), mode 2 intensity progressively increases, reducing the power available to the other modes, until the output power becomes practically constant [region (b)]. In region (c), self-pulsation takes place again and the dominant mode becomes mode 1, while in region (d) the laser is single mode oscillating on mode 0. Finally, region (e) is connected with the self-pulsations taking place in region (a).

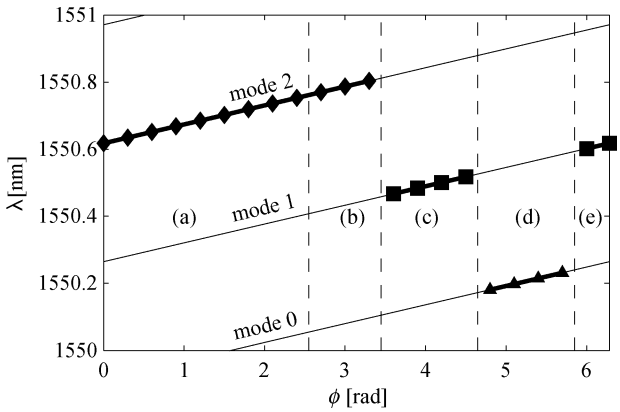

Fig. 9. Spectral position of the modes with the highest power as a function of ϕ. The regions are the same as in Fig. 7 and $\lambda_B = 1550$ nm.

The described alternate behavior between SP and single-mode operation with a strongly detuned emission spectrum respect to the grating Bragg wavelength shows how FWM and longitudinal mode competition determine this fine-tuning characteristic due to current injection in the phase control section.

When using $\alpha_H = 2$, for $I_a = 269$ mA the $P - \phi$ characteristic shows always a single-mode behavior; the lasing mode depends on initial noise conditions (bistability). For $\alpha_H = 6$ (see Fig. 10), the laser is monomode just in a small ϕ interval between 4.6 and 5.7 rad: for all the other ϕ values, it is SP. These results also confirm the fundamental role of the Henry factor α_H and FWM in obtaining self-pulsations.

The above-mentioned procedure can be repeated for all the currents in the range of interest to self-pulsations. As an example, in Fig. 11 a map of the obtained results is reported for the case $\alpha_H = 4$. In the horizontal bars, the information on the ratio between the maximum and minimum instantaneous output power is reported with a gray scale. Dark represents good SP and white single-mode behavior. This map shows how the combination of injection currents in the active section and in the phase control section allows to determine the best SP conditions.

C. Carrier-Instantaneous Frequency Analysis

While looking for self-pulsations, it can be difficult to identify the correct SP behavior of a 3S DBR. The time evolution of the output field and the optical spectrum do not always provide easy

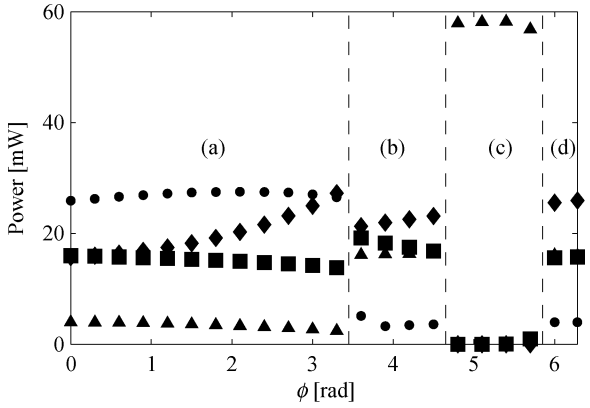

Fig. 10. Mode output power as in Fig. 8 when $\alpha_H = 6$ and $I_a = 269$ mA (▲: mode 0, ■: mode 1, ♦: mode 2, • mode 3). In regions (a), (b), and (d), the device is SP, while in (c) it is monomode.

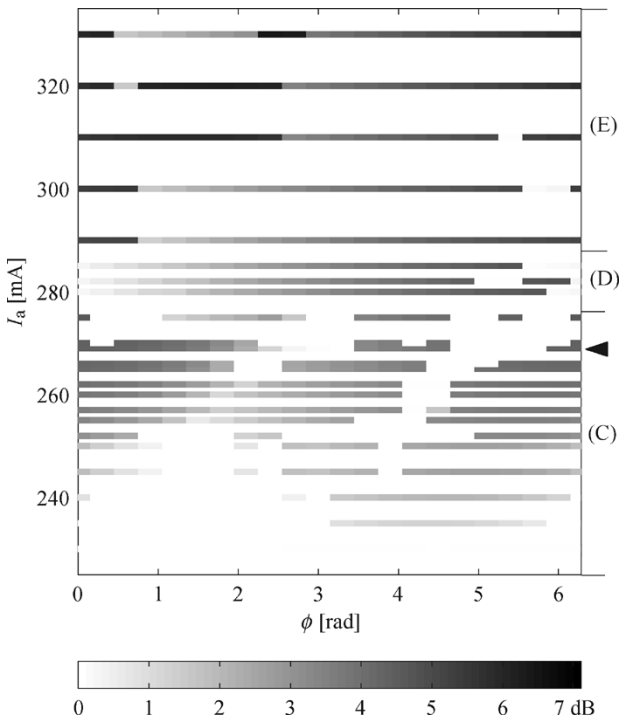

Fig. 11. Ratio between the maximum and the minimum values extracted from the temporal evolution of the output power (in decibels) when $\alpha_H = 4$, for different values of I_a and ϕ. The dark segments on the horizontal bars correspond to better SP conditions, whereas the white bars to CW behavior. Regions (C), (D), and (E) refer to Fig. 2. The arrow (◀) indicates the case with $I_a = 269$ mA presented in Fig. 7.

and sufficient information, particularly when operating conditions start being irregular. It is possible to complete the available information considering the laser dynamics in the carrier density–instantaneous frequency plane. The instantaneous frequency can be evaluated using the procedure proposed in [23]. The procedure is not trivial mainly for the noise due to spontaneous emission when the field is low. This analysis is numerically faster than the spectrum evaluation, because it does not require the computation of Fourier transforms.

The SP behavior obtained for $\alpha_H = 4$ and $I_a = 300$ mA [Fig. 2, region (E)] whose spectrum is reported in Fig. 4 has been analyzed with this technique. Fig. 12 reports the results obtained considering the carrier densities in different points in

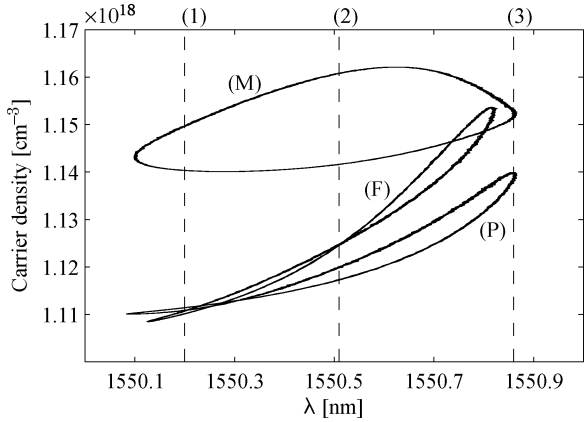

Fig. 12. Periodic pulsations in the carrier density–instantaneous wavelength plane when $\alpha_H = 4$ and $I_a = 300$ mA. The three trajectories are calculated using the carrier density in the middle of the active region (M), near the phase control section (P), and near the cleaved facet (F). The dashed lines indicate the position of modes 1–3 of Fig. 4.

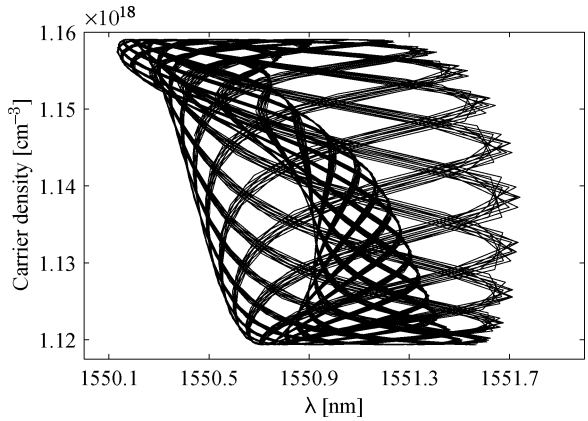

Fig. 13. Representation of quasi-periodic SP in the carrier density–instantaneous wavelength plane when $\alpha_H = 6$ and $I_a = 300$ mA.

the active section of Fig. 1: a point in the middle of the active (curve M), near the phase control (curve P), and at the cleaved facet (curve F). The three trajectories in the carrier-wavelength plane are not identical due to spatial hole burning, but all of them present a limit cycle that indicates a periodic behavior. The cycles touch the wavelength of the three modes having the highest power (modes 1–3 in Fig. 4); the role of FWM is clearly indicated by the detuning respect to the grating Bragg wavelength of 1550 nm. On the contrary, a monomodal operation condition has a trajectory in the plane that is a point.

When the output power begins to be irregular (as for $\alpha_H = 6$, $I_a = 300$ mA, region (D) in Fig. 6) it is possible to see a quasi-periodic behavior (Fig. 13) [24]. This peculiar operating regime can be confirmed also by the examination of the optical spectrum (Fig. 14): additional spectral components with a high power appear, but their spacing is not the FSR.

This analysis allows a fast and effective way to characterize the device dynamics; it regroups on the same plot the information on the operating behavior of the laser, the number and the wavelengths of the modes having the highest power, and the variation of the carrier density in the cavity. Furthermore, this analysis is useful to determine the dynamic conditions when the simulation time has not been long enough or the transient is too

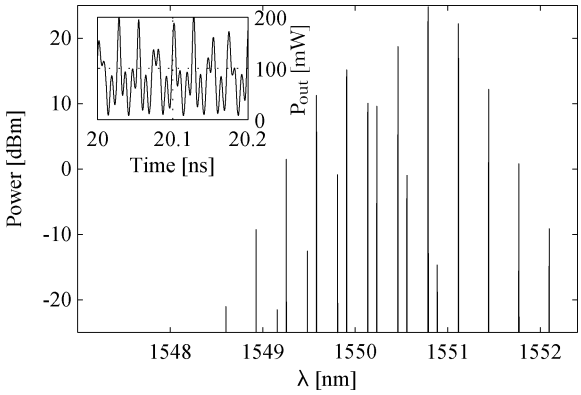

Fig. 14. Laser output signal spectrum for the case in Fig. 13; instantaneous power in the insert.

long. In this case the evolution of the trajectory allows to better predict the steady state behavior.

IV. Conclusion

The full static and dynamic characteristic of 3S DBR laser showing self-pulsation at about 40 GHz has been analyzed changing material parameters and bias conditions. The relevant role of FWM has been clearly shown by the simulation results of the emission spectrum and from the high sensitivity of the device characteristics to the linewidth enhancement factor. A quantitatively good agreement has also been found with the only published experimental results [9] of the optical spectrum of a 3S DBR laser operating in the SP regime.

References

[1] C. Bornholdt, B. Sartorius, S. Schelhase, M. Möhrle, and S. Bauer, "Self-pulsating DFB laser for all-optical clock recovery at 40 Gbit/s," *Electron Lett.*, vol. 36, no. 4, pp. 327–328, Feb. 2000.

[2] B. Sartorius, C. Bornholdt, M. Mohrle, P. Brindel, and O. Leclerc, "System application of 40 GHz all-optical clock in a 40 Gbit/s 3R regenerator," in *Proc. Optical Fiber Communication Conf.*, vol. 4, 2000, pp. 199–201.

[3] W. Mao, X. Wang, X. Al-Mumin, and G. Li, "40 Gb/s all-optical clock recovery using three section sell-pulsation DFB lasers," in *Proc. Optical Fiber Communication Conf.*, vol. 3, 2000, pp. 79–80.

[4] H. Wenzel, U. Bandelow, H. Wünsche, and J. Rehberg, "Mechanisms of fast self pulsations in two-section DFB lasers," *IEEE J. Quantum Electron.*, vol. 32, no. 2, pp. 69–78, Jan. 1996.

[5] A. Vizzino, M. Gioannini, and I. Montrosset, "Dynamic simulation of clock recovery with self-pulsating three-section distributed-feedback lasers," *IEEE J. Quantum Electron.*, vol. 38, no. 12, pp. 1580–1586, Dec. 2002.

[6] X. Wang, S. Pappert, J. Hong, and G. Li, "Spatiotemporal dynamics and high-frequency self-pulsations in two-section distributed feedback lasers," *J. Opt. Soc. Amer. B*, vol. 6, no. 11, pp. 2030–2039, Nov. 1999.

[7] O. Brox, S. Bauer, M. Radziunas, M. Wolfrum, J. Sieber, J. Kreissel, B. Sartorius, and H.-J. Wünsche, "High-frequency pulsations in DFB lasers with amplified feedback," *IEEE J. Quantum Electron.*, vol. 39, no. 11, pp. 1381–1387, Nov. 2003.

[8] M. H. Mourad, J. Vilcot, D. Decoster, and D. Marcenac, "Design and simulation of a dual mode semiconductor laser using sampled grating DFB structure," *IEE Proc. Optoelectron.*, vol. 147, no. 1, pp. 37–42, Feb. 2000.

[9] G.-H. Duan, C. Gosset, B. Lavigne, R. Brenot, B. Thedrez, J. Jacquet, and O. Leclerc, "40 GHz all-optical clock recovery using polarization-insensitive distributed Bragg reflector lasers," in *Proc. 11th Eur. Conf. Integrated Optics (ECIO 2003)*, pp. 175–178.

[10] P. Landais, J. Renaudier, P. Gallion, and G.-H. Duan, "Analysis of self-pulsation in distributed Bragg reflector laser based on four-wave mixing," presented at the SPIE Photonics West Conf., San Jose, CA, 2004.

[11] B.-S. Kim, Y. Chung, and J.-S. Lee, "An efficient split-step time-domain dynamic modeling of DFB/DBR laser diodes," *IEEE J. Quantum Electron.*, vol. 36, no. 7, pp. 787–794, Jul. 2000.

[12] D. J. Jones, L. Zhang, J. Carroll, and D. D. Marcenac, "Dynamics of monolithic passively mode-locked semiconductor lasers," *IEEE J. Quantum Electron.*, vol. 31, no. 6, pp. 1051–1058, Jun. 1995.

[13] D. Syvridis, G. Guekos, S. Pajarola, and M. Tsilis, "Large optical bistability and self pulsations in three section DBR laser diodes," *IEEE Photon. Technol. Lett.*, vol. 6, no. 5, pp. 594–596, May 1994.

[14] A. V. Oppenheim and R. W. Schafer, *Discrete-Time Signal Processing*. Englewood Cliffs, NJ: Prentice-Hall, 1989.

[15] A. P. Bogatov, P. G. Eliseev, and O. G. Okhotnikov, "Interaction of modes and self-stabilization of single-frequency emission of an injected laser with an external selective resonator," *Sov. J. Quantum Electron.*, vol. 13, pp. 1221–1229, 1983.

[16] A. M. Akulsshin *et al.*, "Anomalously wide continuous tuning range of the emission of an injection laser with an external selective resonator," *Sov. J. Quantum Electron.*, vol. 16, pp. 912–918, 1996.

[17] A. P. Bogatov, P. G. Eliseev, and B. N. Sverlov, "Anomalous interaction of spectral modes in a semiconductor laser," *IEEE J. Quantum Electron.*, vol. QE-11, no. 7, pp. 510–515, Jul. 1975.

[18] A. P. Bogatov, P. G. Eliseev, O. Kobildzhanov, and V. Madgazin, "Suppression and spectral splitting of the amplitude noise due to mode beatings in a single-frequency injection laser," *IEEE J. Quantum Electron.*, vol. 23, no. 6, pp. 1064–1070, Jun. 1987.

[19] B. Tromborg, J. Mork, and V. Velinchansky, "On mode coupling and low-frequency fluctuations in external-cavity laser diodes," *Quantum Semiclass. Opt.*, vol. 9, pp. 831–851, 1997.

[20] A. Godard, G. Pauliat, G. Roosen, and E. Ducloux, "Modal competition via four-wave mixing in single-mode extended-cavity semiconductor lasers," *IEEE J. Quantum Electron.*, vol. 40, no. 8, pp. 970–981, Aug. 2004.

[21] A. Godard, G. Pauliat, G. Roosen, P. Graindorge, and P. Martin, "Side-mode gain in grating-tuned extended-cavity semiconductor lasers: investigation of stable single-mode operation conditions," *IEEE J. Quantum Electron.*, vol. 38, no. 4, pp. 390–401, Apr. 2002.

[22] E. Detoma, B. Tromborg, and I. Montrosset, "The complex way to laser diode spectra: example of an external cavity laser with strong optical feedback," *IEEE J. Quantum Electron.*, vol. 41, no. 2, pp. 171–182, Feb. 2005.

[23] B. Boashash, "Estimating and interpreting the instantaneous frequency of a signal—Part 2: Algorithms and applications," *Proc. IEEE*, vol. 80, no. 4, pp. 540–568, Apr. 1992.

[24] J. Guckenheimer and P. Holmes, *Nonlinear Oscillations, Dynamical Systems and Bifurcations of Vector Fields*. New York: Springer-Verlag, 1983.

Paolo Bardella was born in Torino, Italy, in 1977. He received the Laurea degree in electronics from the Politecnico di Torino, Torino, Italy, in 2001. Since 2002, he has been working toward the Ph.D. degree in electronic and communication engineering at the Politecnico di Torino.

His research interests include simulation of multisection semiconductor lasers in the mode-locking and self-pulsating regime.

Ivo Montrosset (M'92) was born in Aosta, Italy, in 1946. He received the Laurea degree in electronic engineering from the Politecnico di Torino, Torino, Italy, in 1971.

From 1972 to 1986, he was with the Politecnico di Torino. In 1986, he was appointed Full Professor at the Universita di Genova, Genova, Italy. Since 1990, he has been Full Professor of Optoelectronics at the Politecnico di Torino. His main activities are in the field of guided wave optics, solid-state and semiconductor lasers, and related topics.

Prof. Montrosset is a Member of IEEE Lasers and Electro-Optics Society (LEOS) and the Optical Society of America (OSA).